Letter

Nonlinear planar Hall effect induced by interband transitions: Application to surface states of topological insulators

Jia-Yan Ba,[1] Yi-Min Wang,[2] Hou-Jian Duan,[1,3] Ming-Xun Deng,[1,3,*] and Rui-Qiang Wang[1,3,†]

[1]*Guangdong Basic Research Center of Excellence for Structure and Fundamental Interactions of Matter, Guangdong Provincial Key Laboratory of Quantum Engineering and Quantum Materials, School of Physics, South China Normal University, Guangzhou 510006, China*

[2]*School of Teacher Education, Guangdong University of Education, Guangzhou 510303, China*

[3]*Guangdong–Hong Kong Joint Laboratory of Quantum Matter, Frontier Research Institute for Physics, South China Normal University, Guangzhou 510006, China*

(Received 9 June 2023; revised 11 October 2023; accepted 21 November 2023; published 11 December 2023)

Motivated by recent experiments observing the nonlinear planar Hall effect (NPHE) in nonmagnetic topological materials, we employ the density matrix method to consider all the intraband and interband transitions. This gives a deeper insight for the different mechanisms of NPHE on the same footing beyond the semiclassical theory. Under broken time-reversal symmetry, besides the usual Berry curvature dipole (BCD) contribution, there exists the quantum metric (QM) induced NPHE, which includes the intrinsic and extrinsic components, and exists even within the band gap. This QM term extends the Berry-connection polarizability (BCP) theory which captures only the intrinsic contribution and cannot be applied to the case with finite scattering and nonzero frequency. Moreover, we reveal that the underlying physics of BCP originates essentially from the combination of three interband transitions (injection, shift, and anomalous), very differently from the BCD which is only contributed by an anomalous mechanism. We compare different mechanisms by calculating the NPHE on the surface states of topological insulators and find that the NPHE from different mechanisms exhibits different dependence on the in-plane magnetic field and the chemical potential. Our theory provides an alternative perspective to understand the complicated lineshapes of the NPHE observed near the Dirac point.

DOI: 10.1103/PhysRevB.108.L241104

Introduction. The planar Hall effect (PHE), manifesting itself as a detectable transverse voltage in response to a magnetic field applied in the plane of the sample and electric current, received great attention in quite a few nonmagnetic topological materials, such as Weyl/Dirac semimetals [1] and three-dimensional topological insulators (TIs) [2–5]. Recently, the PHE was extended to the nonlinear regime, and the nonlinear PHE (NPHE) was experimentally confirmed in several experiments [6–9]. On surface states of TIs, He *et al.* ascribe the NPHE to the conversion of a nonequilibrium spin current into a charge current under the application of an in-plane magnetic field [6,7], and Dyrdal *et al.* attribute it to spin-momentum-locking inhomogeneities [10,11]. Yasuda *et al.* regarded the asymmetric magnon scattering as a possible origin of nonlinear PHE in magnetic TIs [8,9]. Observation of NPHE suggests a convenient and sensitive transport probe of the magnetic proximity effect in magnetic-insulator/TI heterostructures [12]. By breaking the time-reversal symmetry (TRS) of TIs with magnetic doping, the Culcer group [13] identified a new resonant photovoltaic effect and Kim *et al.* [14] reported a pure shift spin current.

The famous nonlinear theory at a low-frequency electric field was proposed by Sodemann and Fu [15], based on the Boltzmann equation, which pointed out that the nonlinear Hall effect (NHE) is related to the nonlinear Drude term arising from the intraband effects and Berry curvature dipole (BCD) from the abnormal velocity induced by Berry curvature (BC). Under TRS but broken inversion symmetry (IS), only the BCD contributes to the NHE. Since BCD-induced NHE is related to topology and geometry property of materials, it receives extensive attention in Weyl semimetals [16–21] and in TIs [22]. The strong NHE appears in anisotropic or tilted bands for noncentrosymmetric transition metal such as WTe_2 [22–24]. When this semiclassical theory is applied to the system with broken TRS, the nonlinear Drude term also explains the unidirectional magnetoresistance [6] or NPHE [7] very well for the chemical potential away from the Dirac point. Nevertheless, when the chemical potential is in the vicinity of the Dirac point, there are many behaviors [12,25] of the NPHE or the unidirectional magnetoresistance that cannot be interpreted even with BCD. Thus, it is highly desirable to revisit the nonlinear-response theory near the Dirac point. In observing the PHE, the applied in-plane magnetic field breaks the TRS. We know that for TRS-broken systems, besides the BCD, there is another electric-field induced interband transition mechanism, namely Berry-connection polarizability (BCP) [26]. The BCP is directly associated with the quantum metric (QM) and has recently received great attention [27–30]. Based on the semiclassical theory, the BCP is derived as an intrinsic second-order correction of an electric field in the dc limit. On the other hand, it is well known that in photocurrents the interband transitions include anomalous, injection, and

*dengmingxun@scnu.edu.cn
†wangruiqiang@m.scnu.edu.cn

shift mechanisms [20,31–35]. The BCD, stemming from the abnormal velocity of wave-packet dynamics in semiclassical theory, essentially originates from the dc-limited anomalous mechanism of interband transitions [20] while the other contributions from the injection and shift mechanisms can be negligible [34–37]. In contrast, which mechanism of interband transitions contributes to the BCP is unknown, and moreover the BCP, capturing only the intrinsic contribution, also cannot be applied to the scattering or finite frequency situation.

In this Letter, we give a deeper insight into the different nonlinear-response mechanisms of NPHE in the nonlinear-response theory by considering all the geometry-related interband transitions near the Dirac point based on the density matrix method. Here, we bridge between dc current (including BCP) and photocurrent, and reveal that the mechanism of BCP originates essentially from the combination of three interband transitions (injection, shift, and anomalous), very differently from the BCD which is only contributed by an anomalous mechanism. We obtain a more general version of the BCP, i.e., Eqs. (7)– (9), which are suitable for arbitrary frequency and finite scattering, extending the BCP based on the classical theory. In the zero frequency and scattering-free case, they reduce to the usual BCP. Using these formulas, we further discuss the NPHE in the vicinity of the Dirac point of the TI surface states. We find that the NPHE due to BCP and BCD conductivities exhibits different dependence on the in-plane magnetic field and chemical potential, from which one can identify BCP mechanism from the others and understand the complicate line shape of the NPHE near the Dirac point.

Theory for second-order nonlinear response. Considering a time dependent but spatially uniform electric field $\mathbf{E}(t) = \mathbf{E}(\omega)e^{-i\omega t} + \text{c.c.}$, the coupling of the light or an alternating electric field can be introduced into the Hamiltonian in the length gauge [38,39]:

$$H(\mathbf{k}, t) = H_0(\mathbf{k}) + e\mathbf{E}(t)\cdot\mathbf{r}, \tag{1}$$

where $H_0(\mathbf{k})$ is the unperturbed Hamiltonian, satisfying $H_0(\mathbf{k})|n\rangle = \epsilon_n|n\rangle$ with $|n\rangle$ being the periodic part of the nth Bloch state. In order to obtain the nonlinear response, we begin with the quantum Liouville equation [34,40], for the density matrix $\rho(t)$, which reads

$$i\hbar\dot{\rho}^{(i)}_{nm}(t) = \epsilon_{nm}\rho^{(i)}_{nm}(t) + [e\mathbf{E}(t)\cdot\mathbf{r}, \rho^{(i-1)}(t)]_{nm} - i\Gamma\rho^{(i)}_{nm}(t). \tag{2}$$

Here, $\epsilon_{nm} = \epsilon_n - \epsilon_m$, and we expand the density matrix in powers of the electric field as $\rho_{nm}(t) = \rho^{(0)}_{nm} + \rho^{(1)}_{nm}(t) + \rho^{(2)}_{nm}(t) + \cdots$, where superscripts indicate the order in the electric field. The equilibrium density matrix is $\rho^{(0)}_{nm} = f_n\delta_{nm}$, where f_n is the equilibrium Fermi-Dirac distribution $f_n = 1/[1 + e^{(\epsilon_n-\mu)/k_BT}]$ with μ the chemical potential and T the temperature. In Eq. (2), we take a simple relaxation time approximation with Γ as the relaxation rate. The complex role of disorders on the nonlinear conductivity is indeed a subject of current intense investigation [41–47], but here we simplify it in order to emphasize the $\mathbf{E}(t)$-induced interband contributions.

Performing the Fourier transformation formation of Eq. (2) and following a standard perturbation theory [38,39,48–51] (see the Supplemental Material [52]), one can obtain the second-order current as $j^{\gamma(2)} = \sum_{\beta\alpha}\sigma^{\gamma;\beta\alpha}(\omega_1,\omega_2)E^{\beta}(\omega_2)E^{\alpha}(\omega_1)$, where $\sigma^{\gamma;\beta\alpha}(\omega_1,\omega_2)$ is the frequency-dependent second-order conductivity tensor. Afterwards, we will focus on the rectified current $\omega_1 = -\omega_2 = \omega$ and the same discussion is suitable for the second harmonic $\omega_1 = \omega_2$. We denote the total conductivity as $\sigma^{\gamma;\beta\alpha}(\omega) = -\frac{e^3}{2\hbar}\int\frac{d\mathbf{k}}{(2\pi)^d}\sigma^{\gamma;\beta\alpha}(\omega,\mathbf{k})$, with $\sigma^{\gamma;\beta\alpha}(\omega,\mathbf{k}) = \sigma^{\gamma;\beta\alpha}_{Dr}(\omega,\mathbf{k}) + \sigma^{\gamma;\beta\alpha}_{an}(\omega,\mathbf{k}) + \sigma^{\gamma;\beta\alpha}_{in}(\omega,\mathbf{k}) + \sigma^{\gamma;\beta\alpha}_{sh}(\omega,\mathbf{k})$, respectively, stemming from the Drude, anomalous, injection, and shift components, where γ is the direction of current and β/α is one of applied electric fields, and d is the dimension of system.

The nonlinear Drude term $\sigma^{\gamma;\beta\alpha}_{Dr}(\omega,\mathbf{k})$, arising from the intraband Fermi-surface shift by $\mathbf{E}(t)$, can expressed with the effective mass $\frac{1}{M^{\beta\gamma}_n} = \frac{\partial}{\partial k_\beta}\frac{\partial\epsilon_n}{\partial k_\gamma}$ as

$$\sigma^{\gamma;\beta\alpha}_{Dr}(\omega,\mathbf{k}) = \sum_n \frac{1}{i\Gamma(\hbar\omega + i\Gamma)}\frac{\partial f_n}{M^{\beta\gamma}_n\partial k_\alpha} + \begin{pmatrix}\alpha\leftrightarrow\beta\\ \omega\leftrightarrow-\omega\end{pmatrix}, \tag{3}$$

where $(\alpha\leftrightarrow\beta, \omega\leftrightarrow-\omega)$ denotes swap of the indices, which can contribute to the longitudinal and Hall currents but vanishes under TRS. For the dc limit, $\sigma^{\gamma;\beta\alpha}_{Dr}$ is dependent on $1/\Gamma^2$.

All the other conductivities including the anomalous $\sigma^{\gamma;\beta\alpha}_{an}(\omega,\mathbf{k})$, injection $\sigma^{\gamma;\beta\alpha}_{in}(\omega,\mathbf{k})$, and shift terms $\sigma^{\gamma;\beta\alpha}_{sh}(\omega,\mathbf{k})$ originate from interband transitions either in the first-order $\rho^{(1)}_{nm}$ or second-order nondiagonal density matrix $\rho^{(2)}_{nm}$. They are related to the non-Abelian Berry connection [38,53] $\mathbf{A}_{nm} = \langle n|i\partial_{\mathbf{k}}|m\rangle$, and can be separated into the band-resolved BC part with $\Omega^{\gamma\beta}_{nm} = i(A^{\gamma}_{nm}A^{\beta}_{mn} - A^{\gamma}_{mn}A^{\beta}_{nm})$ and the band-resolved QM part with $G^{\gamma\beta}_{nm} = \frac{1}{2}(A^{\gamma}_{nm}A^{\beta}_{mn} + A^{\gamma}_{mn}A^{\beta}_{nm})$ [54–56]. For the TRS case, the QM parts vanish and only the BC parts exist, given by (see the Supplemental Material [52])

$$\sigma^{\gamma;\beta\alpha}_{an,BC}(\omega,\mathbf{k}) = \frac{i}{\hbar\omega + i\Gamma}\sum_{m\neq n}\frac{\epsilon^2_{mn}}{\Gamma^2 + \epsilon^2_{nm}}\Omega^{\gamma\beta}_{nm}\frac{\partial f_n}{\partial k_\alpha} + \begin{pmatrix}\alpha\leftrightarrow\beta\\ \omega\leftrightarrow-\omega\end{pmatrix}, \tag{4}$$

$$\sigma^{\gamma;\beta\alpha}_{in,BC}(\omega,\mathbf{k}) = \frac{i}{2}\sum_{n\neq m}\frac{(f_n - f_m)\Omega^{\beta\alpha}_{nm}}{(\hbar\omega - \epsilon_{mn})^2 + \Gamma^2}\frac{\partial\epsilon_{nm}}{\partial k_\gamma} + \begin{pmatrix}\alpha\leftrightarrow\beta\\ \omega\leftrightarrow-\omega\end{pmatrix}, \tag{5}$$

$$\sigma^{\gamma;\beta\alpha}_{sh,BC}(\omega,\mathbf{k}) = -\sum_{n\neq m}\frac{1}{\Gamma^2 + \epsilon^2_{nm}}\frac{i\epsilon_{nm}(f_n - f_m)/2}{(\hbar\omega - \epsilon_{nm})^2 + \Gamma^2} \times\left[\big((\hbar\omega - 2i\Gamma)\epsilon_{nm} - \epsilon^2_{nm} + i\Gamma\hbar\omega\big)Q^{\gamma;\beta\alpha}_{nm} - \frac{i\Gamma\epsilon_{nm}(\hbar\omega - \epsilon_{nm})\Omega^{\gamma\alpha}_{nm}}{\Gamma^2 + \epsilon^2_{nm}}\frac{\partial\epsilon_{nm}}{\partial k_\beta}\right] + \begin{pmatrix}\alpha\leftrightarrow\beta\\ \omega\leftrightarrow-\omega\end{pmatrix}. \tag{6}$$

Here, for $\Gamma, \hbar\omega \ll |\epsilon_{nm}|$, the anomalous conductivity $\sigma^{\gamma;\beta\alpha}_{an,BC}(\omega,\mathbf{k})$ reduces to the famous BCD nonlinear Hall conductivity [15]. Since $\Omega^{\gamma\beta}_{nm}=0$ if $\gamma=\beta$, there is not longitudinal conductivity for $\sigma^{\gamma;\beta\alpha}_{an,BC}(\omega,\mathbf{k})$. The contribution from $\sigma^{\gamma;\beta\alpha}_{in,BC}(\omega,\mathbf{k})$, arising from the difference of band-diagonal electron velocities between empty and occupied states, vanishes for $\omega=0$ due to $\Omega^{\alpha\beta}_{nm}=-\Omega^{\beta\alpha}_{nm}$. $\sigma^{\gamma;\beta\alpha}_{sh,BC}(\omega,\mathbf{k})$ is relevant to the difference between the real-space center of charge for the valence and conduction bands, determined by an extended BC $Q^{\gamma;\beta\alpha}_{nm}=i([D_\gamma A^\beta]_{nm}A^\alpha_{mn}-[D_\gamma A^\beta]_{mn}A^\alpha_{nm})$ with shift vector $[D_\gamma A^\beta]_{nm}=[\frac{\partial}{\partial k_\gamma}-i(A^\gamma_{nn}-A^\gamma_{mm})]A^\beta_{nm}$ [38,39]. $\sigma^{\gamma;\beta\alpha}_{sh,BC}(\omega,\mathbf{k})$ can be negligible at low frequency compared with BCD for $\Gamma, \hbar\omega \ll |\epsilon_{nm}|$. Therefore, for the TRS case, the dominant term is $\sigma^{\gamma;\beta\alpha}_{an,BC}(\omega,\mathbf{k})$ or BCD, in agreement with semiclassical theory [15]. Notice that the BCD in Eq. (4) still provides an extrinsic contribution for NHE.

For the TRS-broken case, except for the contribution from the above BC parts, the anomalous, injection, and shift terms also contribute the current through extra QM-related conductivities, which are derived as (see the Supplemental Material [52])

$$\sigma^{\gamma;\beta\alpha}_{an,QM}(\omega,\mathbf{k})=\frac{-i\Gamma}{\hbar\omega+i\Gamma}\sum_{m\neq n}\frac{2\epsilon_{mn}G^{\gamma\beta}_{nm}}{\Gamma^2+\epsilon^2_{nm}}\frac{\partial f_n}{\partial k_\alpha}+\begin{pmatrix}\alpha\leftrightarrow\beta\\ \omega\leftrightarrow-\omega\end{pmatrix}, \tag{7}$$

$$\sigma^{\gamma;\beta\alpha}_{in,QM}(\omega,\mathbf{k})=\sum_{n\neq m}\frac{-G^{\beta\alpha}_{nm}(f_n-f_m)}{(\hbar\omega-\epsilon_{mn})^2+\Gamma^2}\frac{\partial\epsilon_{nm}}{\partial k_\gamma}+\begin{pmatrix}\alpha\leftrightarrow\beta\\ \omega\leftrightarrow-\omega\end{pmatrix}, \tag{8}$$

$$\sigma^{\gamma;\beta\alpha}_{sh,QM}(\omega,\mathbf{k})=\sum_{n\neq m}\frac{-\epsilon^2_{nm}R^{\gamma;\beta\alpha}_{nm}}{2\left(\Gamma^2+\epsilon^2_{nm}\right)}\frac{(\hbar\omega-\epsilon_{nm}-i\Gamma)(f_n-f_m)}{(\hbar\omega-\epsilon_{nm})^2+\Gamma^2}+\begin{pmatrix}\alpha\leftrightarrow\beta\\ \omega\leftrightarrow-\omega\end{pmatrix}, \tag{9}$$

where we denote an extended QM $R^{\gamma;\beta\alpha}_{nm}=[D_\gamma A^\beta]_{nm}A^\alpha_{mn}+[D_\gamma A^\beta]_{mn}A^\alpha_{nm}$. We can recover those results in Ref. [56] by taking the relaxation rate $\Gamma\to 0$. These QM parts play an important role for the TRS-broken system, especially for the PT-symmetry where the BC parts vanish and only the QM parts survive. One can find that, all QM-related conductivities have both longitudinal and Hall conductivities, which is different from BC-related conductivity. The longitudinal conductivity was also reported by Ref. [13], and should stem essentially from $\sigma^{\gamma;\beta\alpha}_{sh,QM}(\omega,\mathbf{k})$.

In the dc limit, each interband component in Eqs. (7)– (9) has a scattering-independent term, whose summation reads

$$\sigma^{\gamma;\beta\alpha}_{intr,QM}(\omega,\mathbf{k})=-\sum_{m\neq n}\left[\frac{2G^{\gamma\beta}_{nm}}{\epsilon_{mn}}\frac{\partial f_n}{\partial k_\alpha}+\frac{2G^{\beta\alpha}_{nm}f_n}{\epsilon^2_{mn}}\frac{\partial\epsilon_{nm}}{\partial k_\gamma}+\frac{R^{\gamma;\beta\alpha}_{nm}f_n}{\epsilon_{mn}}\right]+(\alpha\leftrightarrow\beta), \tag{10}$$

which originates from the intrinsic components of $\sigma^{\gamma;\beta\alpha}_{an,QM}(\omega,\mathbf{k})$, $\sigma^{\gamma;\beta\alpha}_{in,QM}(\omega,\mathbf{k})$, and $\sigma^{\gamma;\beta\alpha}_{sh,QM}(\omega,\mathbf{k})$ in turn. This intrinsic conductivity is intriguing, in sharp contrast to the extrinsic BC conductivity. It is determined purely by interband Berry connections, which provides a measurable quantum to probe the topological and geometric property of band structure. Recently, in addition to the intraband nonlinear Drude conductivity being used to detect Néel order [57], the nonlinear Hall effects from different sources were also used experimentally to probe various physical quantities. Shao *et al.* [58] used the nonlinear Hall effect caused by the BCD to probe the antiferromagnet Néel vector. Wang *et al.* [27] and the Yang group [28] used the intrinsic Hall effect arising from the BCP to probe the antiferromagnet Néel vector and further to generate the spin polarization [29]. Also, the intrinsic nonlinear planar Hall effect has been proposed [30]. Here, the obtained intrinsic nonlinear conductivity in Eq. (10) can be rewritten as (see the Supplemental Material [52])

$$\sigma^{\gamma;\beta\alpha}_{intr,QM}(\omega,\mathbf{k})=-2\,\mathrm{Re}\sum_{n\neq m}\left(\frac{v^\gamma_n A^\beta_{nm}A^\alpha_{mn}}{\epsilon_n-\epsilon_m}\frac{\partial f_n}{\partial\epsilon_n}-(\beta\leftrightarrow\gamma)\right)+\sum_{n\neq m}\frac{R^{\gamma;\beta\alpha}_{nm}}{\epsilon_{mn}}f_n+(\alpha\leftrightarrow\beta). \tag{11}$$

Compared with previous semiclassical theory with the BCP [26–28], there appears a new term $\sum_{n\neq m}\frac{R^{\gamma;\beta\alpha}_{nm}}{\epsilon_{mn}}f_n$, which could contribute not only the intrinsic Hall conductivity but also the intrinsic longitudinal one.

NPHE in TIs. In order to gain a deeper insight into the QM-induced nonlinear Hall conductivity under broken TRS, we apply the theory to calculate the NPHE on the surface of TIs, which provides a powerful platform to observe the NPHE in recent experiments [12]. Note that in our theory we ignore the orbit effect and so the theory is suitable for anomalous PHE from magnetization-broken TRS or for the two-dimension case with applied in-plane magnetic field. Here, on the surface of TIs, the orbital effect from the in-plane magnetic field can be ignored safely since we can choose the gauge for the vector potential $\mathbf{A}=(0,0,A_z)$. When an in-plane magnetic field $\mathbf{B}=(B_x,B_y)=B[\cos(\theta_B),\sin(\theta_B)]$ is applied to break Kramers degeneracy, the surface state of a three-dimensional TI is modeled with the effective Hamiltonian [59,60]

$$H_{\mathrm{TI}}=\hbar v_F(\sigma_x k_y-\sigma_y k_x)+\frac{\lambda}{2}(k^3_+ +k^3_-)\sigma_z+\mathbf{B}\cdot\boldsymbol{\sigma}, \tag{12}$$

where v_F is the Fermi velocity, $\boldsymbol{\sigma}=(\sigma_x,\sigma_y,\sigma_z)$ is the vector of Pauli matrices acting on real spin, and $k_\pm=k_x\pm ik_y$ with $\mathbf{k}$ being the wave vector. The first term is the Rashba-type spin-orbit coupling and the cubic-in-$\mathbf{k}$ term represents the hexagonal warping effect [61,62] of TIs with the warping parameter λ. In Eq. (12), we have ignored the particle-hole asymmetry term with $\varepsilon_0(\mathbf{k})$, which can lead to the tilt of the energy band under an in-plane magnetic field [4,63], but its contribution $\propto|\mu|$ can be negligible in the vicinity of the Dirac point as considered here. The energy dispersion of the Hamiltonian in Eq. (12) reads

$$\varepsilon^\chi_{\mathbf{k}}=\chi\hbar v_F\sqrt{(k_x-B_y/\hbar v_F)^2+(k_y+B_x/\hbar v_F)^2+\Lambda^2_{\mathbf{k}}}, \tag{13}$$

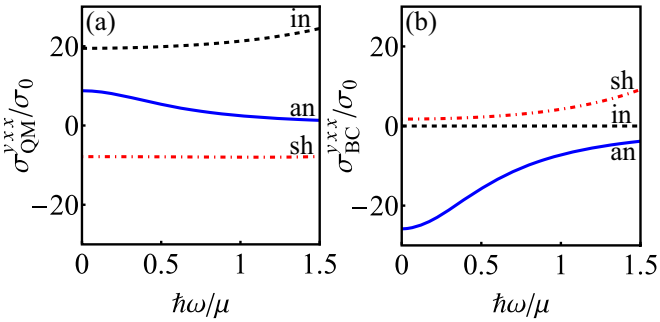

FIG. 1. Interband NPHE at low photon frequency ω. (a) QM-induced anomalous $\sigma^{yxx}_{an,QM}(\omega)$, injection $\sigma^{yxx}_{in,QM}(\omega)$, and shift $\sigma^{yxx}_{sh,QM}(\omega)$, which have comparable magnitudes. (b) BC-induced $\sigma^{yxx}_{an,BC}(\omega)$ dominates while $\sigma^{yxx}_{in,BC}(\omega)$ and $\sigma^{yxx}_{sh,BC}(\omega)$ are negligible small. The conductivity is scaled with $\sigma_0 = e^2/(2\pi)^2\hbar$ nm/V. We choose $\mu = 1.6$ meV, $\Gamma = 1$ meV, magnetic field strength $B = 0.2\hbar v_F \text{nm}^{-1}$, and the angular $\theta_B = \pi/4$. The other parameters of TI material are set as $\hbar v_F = 0.255$ eV nm [59] and $\lambda = 250$ eV Å^3 [60].

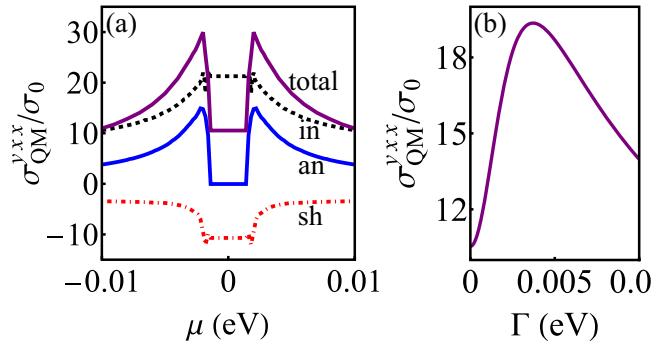

FIG. 2. (a) In the dc case, the dependence of QM-induced intrinsic NPHE on μ with $\Gamma = 0$, which stems from injection, anomalous, and shift interband transitions. (b) The total QM-induced NPHE within the band gap for $\mu = 0$, including the intrinsic and extrinsic components, as a function of the impurity scattering strength Γ. The other parameters are the same as in Fig. 1

where $\Lambda_{\mathbf{k}} = [\lambda k_x(k_x^2 - 3k_y^2)]/(\hbar v_F)$ and $\chi = \pm$ denote the upper and lower bands. In this model, the magnetic field and warping effect break the TRS and mirror symmetry. By coordinate transformation, one can find that the band gap is $E_g = 2|\lambda(B/\hbar v_F)^3 \sin 3\theta_B|$ [64], which implies that the band gap is closed at $\theta_B = n\pi/3$ and opened for the others. In this system, both TRS and IS are broken and the NPHE can originate from Drude, BC, and QM conductivities. It is interesting to distinguish the QM mechanism from the other ones.

We calculate the the nonlinear planar Hall conductivity (NPHC) $\sigma^{\gamma\beta\alpha}(\omega) = -\frac{e^3}{2\hbar}\int \frac{d\mathbf{k}}{(2\pi)^d}\sigma^{\gamma\beta\alpha}(\omega, \mathbf{k})$ assuming an electric field $\mathbf{E} = E^x(\omega)e^{-i\omega t}\hat{\mathbf{x}} + \text{c.c.}$ (corresponding to a linearly polarized light or ac electric field) applied along the x direction. In Fig. 1(a), we plot QM-induced conductivities by three types of interband conductivities at low frequency ω. Obviously, $\sigma^{yxx}_{an,QM}(\omega)$, $\sigma^{yxx}_{in,QM}(\omega)$, and $\sigma^{yxx}_{sh,QM}(\omega)$ have comparable magnitudes. This is different from the BC conductivities shown in Fig. 1(b), where only $\sigma^{yxx}_{an,BC}(\omega)$ dominates at low frequency while $\sigma^{yxx}_{in,BC}(\omega)$ and $\sigma^{yxx}_{sh,BC}(\omega)$ become relatively negligible, recalling the scenario of the TRS case. This implies that under broken TRS, all the interband contributions need to be considered at low frequency, in contrast to the TRS theory [15] where only $\sigma^{yxx}_{an,BC}(\omega)$ or BCD needs to be considered.

In the dc case, we know that the BCD conductivity is extrinsic and proportional to $1/\Gamma$. In contrast, QM-induced conductivities include both intrinsic and extrinsic parts. In order to clarify this, we first calculate the intrinsic NPHC with Eq. (10) and plot QM-induced conductivities as a function of chemical potential μ in Fig. 2(a). The prominent intrinsic NPHC is shown to originate from anomalous, injection, and shift mechanisms, respectively corresponding to the first three terms in Eq. (10). With the decrease of the chemical potential $|\mu|$, all the intrinsic NPHCs increase and exhibit large magnitude as $|\mu|$ approaches the band gap edge, which is caused by rapidly changing QM. From Eq. (10), one can see that anomalous conductivity stems from the contribution of the Fermi surface while injection and shift conductivities are related to the Fermi sea. As a result, even within the band gap, $\sigma^{yxx}_{in,QM}$ and $\sigma^{yxx}_{sh,QM}$ are finite. Despite the opposite sign between $\sigma^{yxx}_{in,QM}$ and $\sigma^{yxx}_{sh,QM}$, there exists a net component in total intrinsic conductivity $\sigma^{yxx}_{intr,QM}$, which is different from previous works [27,28,30] where there is no net intrinsic conductivity in the band gap. This difference is attributed to the new term in Eq. (11). Except for the intrinsic components, there is an extrinsic one which is entangled with the intrinsic one arising from the interband coherence, as seen from Eqs. (7)– (9) with $\omega = 0$. In Fig. 2(b), we show that the total QM-induced NPHC σ^{yxx}_{QM} is nonmonotonically enhanced by the scattering strength Γ.

The in-gap current has received attention in earlier years [65–68]. Some prominent studies [69,70] concluded that such rectification within the optical gap is impossible in the clean limit. On the other hand, some recent studies [46,47], starting from the full quantum mechanical description, showed that the in-gap rectification can actually be real and thermodynamically allowed. Notice that these reports about the in-gap current originate from mechanisms that are very different from the ones here. It is interesting to make a comparison. (1) The in-gap rectification in works [46,47] is defined in the so-called optical gap, namely the frequency is located in $\Gamma < \omega < \Delta$ (where Δ stands for the band gap) and the Fermi surface is in the conduction or valence band. This is purely the Fermi-surface contribution, determined by the Fermi-surface characteristics, such as the specific form of the Fermi distribution function. It is just these rich Fermi-surface behaviors that lead to the interesting in-gap rectification, beyond the simple relaxation approximation. (2) In contrast, in our Letter, the in-gap current is defined in the case of the Fermi energy being strictly within the band gap. Notice that the QM terms include the contributions from both the Fermi surface and the Fermi sea. Within the band gap, only the Fermi-sea contribution survives, which is just the origin of the in-gap current, insensitive to the Fermi-surface behaviors. This specular photocurrent is the consequence of a parity-violating magnet [56,71]. It is noticed that the in-gap current will vanish if one takes the adiabatic turning-on regularization as in Ref. [72], where $1/(\omega_1 + \omega_2 - \epsilon_{nm} + i2\Gamma)$ is adopted. Compared with the relaxation time approximation,

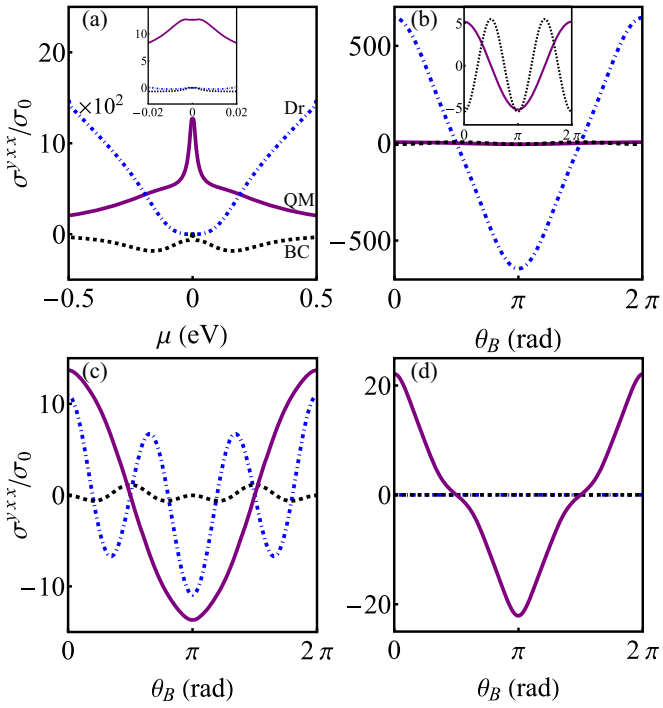

FIG. 3. The variation of the dc NPHC σ^{yxx}_{QM}, σ^{yxx}_{BC}, and σ^{yxx}_{Dr} vs (a) chemical potential μ with $\theta_B = \pi/5$, and vs (b)–(d) θ_B. In (b) $\mu = 0.2$ eV, (c) $\mu = 0.01$ eV slightly out of the band gap, and (d) $\mu = 0$ eV within the band gap. The insets in (a) and (b) are the corresponding enlarged views. We set $\Gamma = 0.02$ eV and the other parameters are the same as in Fig. 1.

there is a discrepancy of a factor 2 in the relaxation rate, which will lead to the compensated in-gap rectification by the principal parts of the diagonal and off-diagonal density matrix elements. Nevertheless, the authors in Refs. [71,73] pointed out that the relaxation rate η of two photons is in general not equal to the double Γ of one photon, namely $\eta \neq 2\Gamma$, and so the in-gap current emerges. Setting $\eta = 2\Gamma$ is just a particular case. Here, we cannot judge which result is correct. Since we employ the simple relaxation time approximation, the in-gap current might be an artifact, which deserves further consideration.

In practice materials, the measured total NPHC can originate from σ^{yxx}_{QM} including intrinsic and extrinsic parts, σ^{yxx}_{BC}, and σ^{yxx}_{Dr}, and it is interesting to distinguish these different mechanisms. In Fig. 3(a), we illustrate the dependence of the NPHCs σ^{yxx}_{QM}, σ^{yxx}_{BC}, and σ^{yxx}_{Dr} on chemical potential μ. For μ far away from the Dirac point, the NPHC σ^{yxx}_{Dr} dominates and exhibits the lineshape of cosinelike function of θ_B with 2π period as shown in Fig. 3(b). This recalls the results obtained in a recent experiment [7], which is interpreted as the conversion of spin current into a charge current. With μ reduced close to the Dirac point, σ^{yxx}_{Dr} decays as shown in Fig. 3(a), where σ^{yxx}_{QM} and σ^{yxx}_{BC} play a dominant role. Differently, as shown in Fig. 3(c), σ^{yxx}_{BC} exhibits a π period while σ^{yxx}_{QM} and σ^{yxx}_{Dr} have 2π period. The reason is that the former scales with $\mathbf{B}^2$ while the latter scale with the order of $\mathbf{B}$. Obviously, their line shape departs from a sinusoidal or cosine function. Near the Dirac point, the interplay of the in-plane $\mathbf{B}$ and the hexagonal warping leads to the $\pi/3$-period band gap, which modulates the period of the planar Hall effect. The relative magnitude between QM and BC contributions is determined mainly by the scattering strength Γ. When μ is located within the band gap, only σ^{yxx}_{QM} survives and its dependence on θ_B of the magnetic field is depicted in Fig. 3(d). In this situation, σ^{yxx}_{Dr} and σ^{yxx}_{BC} vanish due to Fermi surface property and only σ^{yxx}_{QM} survives.

Discussion and conclusions. There are many papers discussing the second-order nonlinear current with the BCP in the framework of semiclassical theory, such as Refs. [26–30]. Notice that the BCP theory can only apply to the dc limit $\omega = 0$ with $\Gamma = 0$. In these works, the BCP is shown to originate from interband transitions but cannot be related to which interband mechanisms it belongs to, such as well known injection and shift. On the other hand, the photocurrent formulas usually diverge [56] as $J \sim 1/\omega$, which cannot directly extend to the dc limit. In this Letter, we present a general formula ranging from zero to high frequency, which bridges between dc current and photocurrent. We find that for $\omega \gg \Gamma$, all formulas can recover the results of the photoncurrent rectification for shift and injection [31,56]. For the low-frequency $\omega \ll \Gamma$ or dc limit, our theory under T-symmetry, where all the BC parts vanish and only anomalous current survives, reduces to the BCD theory [15], and under the PT-symmetry situation both shift and injection currents still remain finite even in $\Gamma = \omega = 0$, which leads to the intrinsic dc component, recovering the BCP results [26–30] except for the extra term in Eq. (11).

In summary, we have investigated the NPHE on the surface of a three-dimensional TI. As the chemical potential μ is far away from the Dirac point, the observed NPHE is caused by the intraband transitions and is interpreted as the conversion of spin current into a charge current [7] . Nevertheless, in the vicinity of the Dirac point, the complicated interband transitions, which have topological geometric origin, make it difficult to describe with the semiclassical theory. The extensively employed semiclassical BCD theory [15] is suitable only for nonmagnetic materials with TRS. In order to study NPHE where the in-plane magnetic field breaks the TRS, we employ a more general nonlinear-response theory by considering all the intraband and interband transitions based on the density matrix method. We find that besides the BCD contribution which requires the band gap opening (here caused by the interplay of in-plane magnetic field and warping effect), we obtain the QM-induced NPHE including the intrinsic and extrinsic components, regardless of the band gap and existing even within the band gap. This QM term extends the BCP theory which captures only the intrinsic contribution and cannot be applied to the case with finite scattering and nonzero frequency. Furthermore, we reveal that the underlying physics of BCP originates essentially from the combination of three interband transitions (injection, shift, and anomalous). We compare different mechanisms by calculating the NPHE on the surface states of TIs and find that the NPHE from different mechanisms exhibits different dependence on the in-plane magnetic field and the chemical potential. All of these provide significant signatures to identify QM from other Drude or BC mechanisms in experiment, and their interplay is helpful for understanding the NPHE near the Dirac point.

Acknowledgments. This work was supported by the National Natural Science Foundation of China (Grants No. 12174121, No. 12104167, and No. 12274146), by the Guangdong NSF of China (Grant No. 2021A1515010369), and by Guangdong Basic and Applied Basic Research Foundation (Grants No. 2020A1515111035 and No. 2023B1515020050).

J.-Y.B. and Y.-M.W. contributed equally to this work.

[1] S. Nandy, G. Sharma, A. Taraphder, and S. Tewari, Chiral anomaly as the origin of the planar Hall effect in Weyl semimetals, Phys. Rev. Lett. **119**, 176804 (2017).

[2] A. A. Taskin, H. F. Legg, F. Yang, S. Sasaki, Y. Kanai, K. Matsumoto, A. Rosch, and Y. Ando, Planar Hall effect from the surface of topological insulators, Nat. Commun. **8**, 1340 (2017).

[3] B. Wu, X. C. Pan, W. Wu, F. Fei, B. Chen, Q. Liu, H. Bu, L. Cao, F. Song, and B. Wang, Oscillating planar Hall response in bulk crystal of topological insulator Sn doped $Bi_{1.1}Sb_{0.9}Te_2S$, Appl. Phys. Lett. **113**, 011902 (2018).

[4] S. H. Zheng, H. J. Duan, J. K. Wang, J. Y. Li, M. X. Deng, and R. Q. Wang, Origin of planar Hall effect on the surface of topological insulators: Tilt of Dirac cone by an in-plane magnetic field, Phys. Rev. B **101**, 041408(R) (2020).

[5] W. Rao, Y. L. Zhou, Y. j. Wu, H. J. Duan, M. X. Deng, and R.-Q. Wang, Theory for linear and nonlinear planar Hall effect in topological insulator thin films, Phys. Rev. B **103**, 155415 (2021).

[6] P. He, S. S. L. Zhang, D. Zhu, Y. Liu, Y. Wang, J. Yu, G. Vignale, and H. Yang, Bilinear magnetoelectric resistance as a probe of three-dimensional spin texture in topological surface states, Nat. Phys. **14**, 495 (2018).

[7] P. He, S. S. L. Zhang, D. Zhu, S. Shi, O. G. Heinonen, G. Vignale, and H. Yang, Nonlinear planar Hall effect, Phys. Rev. Lett. **123**, 016801 (2019).

[8] K. Yasuda, A. Tsukazaki, R. Yoshimi, K. S. Takahashi, M. Kawasaki, and Y. Tokura, Large unidirectional magnetoresistance in a magnetic topological insulator, Phys. Rev. Lett. **117**, 127202 (2016).

[9] K. Yasuda, A. Tsukazaki, R. Yoshimi, K. Kondou, K. S. Takahashi, Y. Otani, M. Kawasaki, and Y. Tokura, Current-nonlinear Hall effect and spin-orbit torque magnetization switching in a magnetic topological insulator, Phys. Rev. Lett. **119**, 137204 (2017).

[10] A. Dyrdał, J. Barnaś, and A. Fert, Spin-momentum-locking inhomogeneities as a source of bilinear magnetoresistance in topological insulators, Phys. Rev. Lett. **124**, 046802 (2020).

[11] A. N. Zarezad, J. Barnaś, A. Qaiumzadeh, and A. Dyrdał, Bilinear planar Hall effect in topological insulators due to spin-momentum locking inhomogeneity, Phys. Status Solidi RRL2200483 (2023).

[12] Y. Wang, S. V. Mambakkam, Y. X. Huang, Y. Wang, Y. Ji, C. Xiao, S. A. Yang, S. A. Law, and J. Q. Xiao, Observation of nonlinear planar Hall effect in magnetic-insulator-topological-insulator heterostructures, Phys. Rev. B **106**, 155408 (2022).

[13] P. Bhalla, A. H. MacDonald, and D. Culcer, Resonant photovoltaic effect in doped magnetic semiconductors, Phys. Rev. Lett. **124**, 087402 (2020).

[14] K. W. Kim, T. Morimoto, and N. Nagaosa, Shift charge and spin photocurrents in Dirac surface states of topological insulator, Phys. Rev. B **95**, 035134 (2017).

[15] I. Sodemann and L. Fu, Quantum nonlinear Hall effect induced by Berry curvature dipole in time-reversal invariant materials, Phys. Rev. Lett. **115**, 216806 (2015).

[16] Y. Zhang, Y. Sun, and B. Yan, Berry curvature dipole in Weyl semimetal materials: An *ab initio* study, Phys. Rev. B **97**, 041101(R) (2018).

[17] C.-L. Zhang, T. Liang, Y. Kaneko, N. Nagaosa, and Y. Tokura, Giant Berry curvature dipole density in a ferroelectric Weyl semimetal, Npj Quantum Mater. **7**, 103 (2022).

[18] C. Zeng, S. Nandy, and S. Tewari, Nonlinear transport in Weyl semimetals induced by Berry curvature dipole, Phys. Rev. B **103**, 245119 (2021).

[19] T. Morimoto, S. Zhong, J. Orenstein, and J. E. Moore, Semiclassical theory of nonlinear magneto-optical responses with applications to topological Dirac/Weyl semimetals, Phys. Rev. B **94**, 245121 (2016).

[20] Z. Li, Y.-Q. Jin, T. Tohyama, T. Iitaka, J.-X. Zhang, and H. Su, Second harmonic generation in the Weyl semimetal TaAs from a quantum kinetic equation, Phys. Rev. B **97**, 085201 (2018).

[21] Y. Gao, F. Zhang, and W. Zhang, Second-order nonlinear Hall effect in Weyl semimetals, Phys. Rev. B **102**, 245116 (2020).

[22] S. Y. Xu, Q. Ma, H. Shen, V. Fatemi, S. Wu, T.-R. Chang, G. Chang, A. M. M. Valdivia, C.-K. Chan, Q. D. Gibson, J. Zhou, Z. Liu, K. Watanabe, T. Taniguchi, H. Lin, R. J. Cava, L. Fu, N. Gedik, and P. Jarillo-Herrero, Electrically switchable Berry curvature dipole in the monolayer topological insulator WTe_2, Nat. Phys. **14**, 900 (2018).

[23] K. Kang, T. Li, E. Sohn, J. Shan, and K. F. Mak, Nonlinear anomalous Hall effect in few-layer WTe_2, Nat. Mater. **18**, 324 (2019).

[24] Z. Z. Du, C. M. Wang, H. Z. Lu, and X. C. Xie, Band signatures for strong nonlinear Hall effect in bilayer WTe_2, Phys. Rev. Lett. **121**, 266601 (2018).

[25] D. Rakhmilevich, F. Wang, W. Zhao, M. H. W. Chan, J. S. Moodera, C. Liu, and C.-Z. Chang, Unconventional planar Hall effect in exchange-coupled topological insulator–ferromagnetic insulator heterostructures, Phys. Rev. B **98**, 094404 (2018).

[26] Y. Gao, S. A. Yang, and Q. Niu, Field induced positional shift of bloch electrons and its dynamical implications, Phys. Rev. Lett. **112**, 166601 (2014).

[27] C. Wang, Y. Gao, and D. Xiao, Intrinsic nonlinear Hall effect in antiferromagnetic tetragonal CuMnAs, Phys. Rev. Lett. **127**, 277201 (2021).

[28] H. Liu, J. Zhao, Y. X. Huang, W. Wu, X. L. Sheng, C. Xiao, and S. A. Yang, Intrinsic second-order anomalous Hall effect and its application in compensated antiferromagnets, Phys. Rev. Lett. **127**, 277202 (2021).

[29] C. Xiao, H. Liu, W. Wu, H. Wang, Q. Niu, and S. A. Yang, Intrinsic nonlinear electric spin generation in centrosymmetric magnets, Phys. Rev. Lett. **129**, 086602 (2022).

[30] Y. X. Huang, X. Feng, H. Wang, C. Xiao, and S. A. Yang, Intrinsic nonlinear planar Hall effect, Phys. Rev. Lett. **130**, 126303 (2023).

[31] H. Wang and X. Qian, Electrically and magnetically switchable nonlinear photocurrent in *PT*-symmetric magnetic topological quantum materials, Npj Comput. Mater. **6**, 199 (2020).

[32] L. Wu, S. Patankar, T. Morimoto, N. L. Nair, E. Thewalt, A. Little, J. G. Analytis, J. E. Moore, and J. Orenstein, Giant anisotropic nonlinear optical response in transition metal monopnictide Weyl semimetals, Nat. Phys. **13**, 350 (2017).

[33] Q. Ma, S.-Y. Xu, C.-K. Chan, C.-L. Zhang, G. Chang, Y. Lin, W. Xie, T. Palacios, H. Lin, S. Jia, P. A. Lee, P. Jarillo-Herrero, and N. Gedik, Direct optical detection of Weyl fermion chirality in a topological semimetal, Nat. Phys. **13**, 842 (2017).

[34] O. Matsyshyn and I. Sodemann, Nonlinear Hall acceleration and the quantum rectification sum rule, Phys. Rev. Lett. **123**, 246602 (2019).

[35] O. Matsyshyn, F. Piazza, R. Moessner, and I. Sodemann, Rabi regime of current rectification in solids, Phys. Rev. Lett. **127**, 126604 (2021).

[36] Q. Ma, S.-Y. Xu, H. Shen, D. MacNeill, V. Fatemi, T.-R. Chang, A. M. M. Valdivia, S. Wu, Z. Du, C.-H. Hsu, S. Fang, Q. D. Gibson, K. Watanabe, T. Taniguchi, R. J. Cava, E. Kaxiras, H.-Z. Lu, H. Lin, L. Fu, N. Gedik *et al.*, Observation of the nonlinear Hall effect under time-reversal-symmetric conditions, Nature (London) **565**, 337 (2019).

[37] F. de Juan, A. G. Grushin, T. Morimoto, and J. E. Moore, Quantized circular photogalvanic effect in Weyl semimetals, Nat. Commun. **8**, 15995 (2017).

[38] C. Aversa and J. E. Sipe, Nonlinear optical susceptibilities of semiconductors: Results with a length-gauge analysis, Phys. Rev. B **52**, 14636 (1995).

[39] J. E. Sipe and A. I. Shkrebtii, Second-order optical response in semiconductors, Phys. Rev. B **61**, 5337 (2000).

[40] R. K. Malla, A. Saxena, and W. J. M. Kort-Kamp, Emerging nonlinear Hall effect in Kane-Mele two-dimensional topological insulators, Phys. Rev. B **104**, 205422 (2021).

[41] H. Isobe, S.-Y. Xu, and L. Fu, High-frequency rectification via chiral Bloch electrons, Sci. Adv. **6**, eaay2497 (2020).

[42] Z. Z. Du, C. M. Wang, S. Li, H.-Z. Lu, and X. C. Xie, Disorder-induced nonlinear Hall effect with time-reversal symmetry, Nat. Commun. **10**, 3047 (2019).

[43] C. Xiao, Z. Z. Du, and Q. Niu, Theory of nonlinear Hall effects: Modified semiclassics from quantum kinetics, Phys. Rev. B **100**, 165422 (2019).

[44] E. J. König, M. Dzero, A. Levchenko, and D. A. Pesin, Gyrotropic Hall effect in Berry-curved materials, Phys. Rev. B **99**, 155404 (2019).

[45] S. Nandy and I. Sodemann, Symmetry and quantum kinetics of the nonlinear Hall effect, Phys. Rev. B **100**, 195117 (2019).

[46] O. Matsyshyn, J. C. W. Song, I. S. Villadiego, and L.-k. Shi, Fermi-Dirac staircase occupation of Floquet bands and current rectification inside the optical gap of metals: An exact approach, Phys. Rev. B **107**, 195135 (2023).

[47] L.-K. Shi, O. Matsyshyn, J. C. W. Song, and I. S. Villadiego, Berry-dipole photovoltaic demon and the thermodynamics of photocurrent generation within the optical gap of metals, Phys. Rev. B **107**, 125151 (2023).

[48] D. E. Parker, T. Morimoto, J. Orenstein, and J. E. Moore, Diagrammatic approach to nonlinear optical response with application to Weyl semimetals, Phys. Rev. B **99**, 045121 (2019).

[49] F. Hipolito, T. G. Pedersen, and V. M. Pereira, Nonlinear photocurrents in two-dimensional systems based on graphene and boron nitride, Phys. Rev. B **94**, 045434 (2016).

[50] H. Watanabe and Y. Yanase, Nonlinear electric transport in odd-parity magnetic multipole systems: Application to Mn-based compounds, Phys. Rev. Res. **2**, 043081 (2020).

[51] Y. Liu, Z. G. Zhu, and G. Su, Photogalvanic effect and second harmonic generation from radio to infrared region in WTe_2 monolayer, arXiv:2302.08103.

[52] See Supplemental Material at http://link.aps.org/supplemental/10.1103/PhysRevB.108.L241104 for a detailed derivation of the second-order conductivity.

[53] E. I. Blount, Formalisms of band theory, Solid State Phys. **13**, 305 (1962).

[54] M. V. Berry, Quantal phase factors accompanying adiabatic changes, Proc. R. Soc. London A **392**, 45 (1984).

[55] J. P. Provost and G. Vallee, Riemannian structure on manifolds of quantum states, Commun. Math. Phys. **76**, 289 (1980).

[56] H. Watanabe and Y. Yanase, Chiral photocurrent in parity-violating magnet and enhanced response in topological antiferromagnet, Phys. Rev. X **11**, 011001 (2021).

[57] W. Chen, M. Gu, J. Li, P. Wang, and Q. Liu, Role of hidden spin polarization in nonreciprocal transport of antiferromagnets, Phys. Rev. Lett. **129**, 276601 (2022).

[58] D. F. Shao, S. H. Zhang, G. Gurung, W. Yang, and E. Y. Tsymbal, Nonlinear anomalous Hall effect for Néel vector detection, Phys. Rev. Lett. **124**, 067203 (2020).

[59] Y. L. Chen, J. G. Analytis, J.-H. Chu, Z. K. Liu, S.-K. Mo, X. L. Qi, H. J. Zhang, D. H. Lu, X. Dai, Z. Fang, S. C. Zhang, I. R. Fisher, Z. Hussain, and Z.-X. Shen, Experimental realization of a three-dimensional topological insulator, Bi_2Te_3, Science **325**, 178 (2009).

[60] L. Fu, Hexagonal warping effects in the surface states of the topological insulator Bi_2Te_3, Phys. Rev. Lett. **103**, 266801 (2009).

[61] R. S. Akzyanov and A. L. Rakhmanov, Surface charge conductivity of a topological insulator in a magnetic field: The effect of hexagonal warping, Phys. Rev. B **97**, 075421 (2018).

[62] R. S. Akzyanov and A. L. Rakhmanov, Bulk and surface spin conductivity in topological insulators with hexagonal warping, Phys. Rev. B **99**, 045436 (2019).

[63] T. Nag, S. K. Das, C. Zeng, and S. Nandy, Third-order Hall effect in the surface states of a topological insulator, Phys. Rev. B **107**, 245141 (2023).

[64] Z.-J. Weng, J.-Y. Ba, Y.-H. Ke, H.-J. Duan, M.-X. Deng, and R.-Q. Wang, Magnon scattering modulated planar Hall effect in a ferromagnet/topological insulator heterostructure, Phys. Rev. B **106**, 195134 (2022).

[65] W. Kraut and R. von Baltz, Anomalous bulk photovoltaic effect in ferroelectrics: A quadratic response theory, Phys. Rev. B **19**, 1548 (1979).

[66] V. I. Belinicher and B. I. Sturman, The photogalvanic effect in media lacking a center of symmetry, Sov. Phys. Usp. **23**, 199 (1980).

[67] R. von Baltz and W. Kraut, Theory of the bulk photovoltaic effect in pure crystals, Phys. Rev. B **23**, 5590 (1981).

[68] V. I. Belinicher, E. L. Ivchenko, and B. I. Sturman, Kinetic theory of the displacement photovoltaic effect in piezoelectrics, Zh. Eksp. Teor. Fiz. **83**, 649 (1982) [Sov. Phys. JETP **56**, 359 (1982)].

[69] V. I. Belinicher, E. L. Ivchenko, and G. E. Pikus, Transient photocurrent in gyrotropic crystals, Sov. Phys. Semicond. **20**, 558 (1986).

[70] E. L. Ivchenko, Y. B. Lyanda-Geller, and G. E. Pikus, Magneto-photogalvanic effects in noncentrosymmetric crystals, Ferroelectrics **83**, 19 (1988).

[71] D. Kaplan, T. Holder, and B. Yan, Nonvanishing subgap photocurrent as a probe of lifetime effects, Phys. Rev. Lett. **125**, 227401 (2020).

[72] L. Gao, Z. Addison, E. J. Mele, and A. M. Rappe, Intrinsic Fermi-surface contribution to the bulk photovoltaic effect, Phys. Rev. Res. **3**, L042032 (2021).

[73] D. Kaplan, T. Holder, and B. Yan, Unifying semiclassics and quantum perturbation theory at nonlinear order, SciPost Phys. **14**, 082 (2023).